Joint Estimation of Current Maps in Quantum Diamond Magnetometry

Prabhat Anand
TCS Research
Tata Consultancy Services Ltd
Bengaluru, India
anand.prabhat@tcs.com

Pavan Kumar Reddy K
TCS Research
Tata Consultancy Services Ltd
Bengaluru, India
pavank.reddy@tcs.com

Anuj Bathla
Department of Electrical Engineering
Indian Institute Technology Bombay
Mumbai, India
bathla.anuj@iitb.ac.in

Kasturi Saha
Department of Electrical Engineering
Indian Institute Technology Bombay
Mumbai, India
kasturis@ee.iitb.ac.in

M Girish Chandra
TCS Research
Tata Consultancy Services Ltd
Bengaluru, India
m.gchandra@tcs.com

***Abstract*—With the importance of signal processing in the next-generation quantum-enhanced sensing systems firmly established in recent times, this paper considers one of the mature quantum sensing technologies: NV centers-based magnetometry. Focusing on the two-dimensional current-carrying structures, we propose a novel joint optimization formulation to obtain current maps (images) considering all the components of the magnetic field vector map along with physical constraints, which facilitate de-convolution required in the processing. The paper systematically works out the necessary algorithmic steps and captures the typical results obtained on both synthetic and real data to bring out the effectiveness of the technique in overcoming the challenges faced by traditional methods.**

***Index Terms*—joint optimization, image reconstruction, magnetometry, ADMM, plug-and-play method**

I. Introduction

Quantum-enhanced sensing, with its ability to bring new and enhanced capabilities compared to classical sensors, is expected to create a significant impact in many industries [1], [2]. Compared to other quantum technologies, the benefits can be reaped in the short term with quantum sensors. Needless to say, similar to their classical counterparts, quantum sensors should move towards sensing systems with the tandem working of the rightly designed hardware and software to exploit their full potential. Some of the core software modules in quantum sensing are related to signal processing and the associated algorithms. As remarked in our earlier work [3], which examined magnetic field construction in the negatively charged nitrogen-vacancy (NV) color centers-based magnetometers, there is a possibility to view the problem of obtaining the requisite outputs through the lens of signal processing. In the current work, we reconsider current maps reconstruction from the magnetic fields maps measured by a vector magnetometer pertaining to its non-invasive measurements of ambient magnetic fields with high spatial resolution and high sensitivity. Even for two-dimensional (2-D) sources, these reconstruction problems are generally ill-conditioned inverse problems [4]–[6], necessitating complex techniques for source retrieval.

To elaborate this, let $\boldsymbol{B}(x, y, z)$ be magnetic field at a given point in space $\boldsymbol{r} = (x, y, z)$ that is related to its current sources $\boldsymbol{J}(x', y', z')$ situated at points $\boldsymbol{r}' = (x', y', z')$ bound to a volume $\Omega = L \times L \times d$ through the Biot Savart law

$$\boldsymbol{B}(\boldsymbol{r}) = \frac{\mu_0}{4\pi} \int_{\Omega} \frac{\boldsymbol{J}(\boldsymbol{r}') \times (\boldsymbol{r} - \boldsymbol{r}')}{|\boldsymbol{r} - \boldsymbol{r}'|^3} d^3\boldsymbol{r}' \tag{1}$$

where μ_0 is the permeability of free space. When we constrain our sources and measurements in a plane with an area of $L \times L$, parallelly placed to each other at a stand-off distance of z_0 s.t. $d \ll L$ and $d \ll z_0$, then we can assume that the flow is purely two-dimensional and thus $\boldsymbol{J} = (J_x, J_y, 0)$, for all practical purposes. This facilitates us a simpler version of (1) where magnetic field components $(B_x,\ B_y,\ B_z)$ are related to the convolution of planar current density with corresponding Green's functions.

$$\begin{aligned} B_x &= \frac{\mu_0}{4\pi} \int \frac{z_0\ J_y(x', y')}{[(x - x')^2 + (y - y')^2 + z_0^2]^{3/2}} dx'dy' \\ &= G_3 * J_y \end{aligned} \tag{2}$$

$$\begin{aligned} B_y &= \frac{\mu_0}{4\pi} \int \frac{-z_0\ J_x(x', y')}{[(x - x')^2 + (y - y')^2 + z_0^2]^{3/2}} dx'dy' \\ &= -G_3 * J_x \end{aligned} \tag{3}$$

$$\begin{aligned} B_z &= \frac{\mu_0}{4\pi} \int \frac{(y - y')\ J_x(x', y') - (x - x')\ J_y(x', y')}{[(x - x')^2 + (y - y')^2 + z_0^2]^{3/2}} dx'dy' \\ &= G_1 * J_x - G_2 * J_y \end{aligned} \tag{4}$$

where $*$ denotes 2-D convolution operation, G_i where $i \in \{1, 2, 3\}$ are kernels corresponding to the Green's functions, and the integral is bounded by the area of the current source $L \times L$. Note that the coordinate dependence of the magnetic field has been suppressed for clarity. Adding the continuity equation in charge-free region ($\nabla . \boldsymbol{J} = 0$) to this gives a set of four integral equations that relate $\boldsymbol{B}$ to $\boldsymbol{J}$. These variables and associated relations in the continuous domain are uniformly

discretized for numerical computations, and in the following, we consider their discrete versions only. We transform the continuous equations into matrix forms where the discretized Green's function kernels can be identified as discrete filters.

The aim of the 2-D current reconstruction is to deconvolve the magnetic field maps to obtain $J_x,\ J_y \in \mathbb{R}^{N\times N}$ using known Green's function filters in (2)-(4). Naively using Fourier inverse filtering [2], [4], [5] in the process to estimate the current density lead to a huge noise amplification in the image as can be inferred from inverse equation in Discrete Fourier Transform (DFT) domain (5).

$$\mathcal{F}\{J_{(y/x)}\} = \frac{\mathcal{F}\{B_{(x/y)}\}}{\mathcal{F}\{\pm G_3\}} = \pm\frac{2}{\mu_0}\exp\left(z_0\sqrt{k_x^2+k_y^2}\right) b_{(x/y)} \tag{5}$$

where $\mathcal{F}\{\cdot\}$ represents the DFT operation and k_x and k_y are the components of discrete spatial frequency and exp denotes element-wise exponentiation. Note in (5), that $J_{y/x}$ is related to $b_{x/y}$ through a high-pass filter which amplifies the high frequency components exponentially more than low frequency components, present in the magnetic field. And since any noise and other sharp artifacts have support on these high frequency components, with increasing z_0, they contribute increasingly in the deconvolution, introducing a huge solution space [6].

To constrain the infinitely large solution space of the under-determined system, appropriate regularizers are often used [6]. But these methods are not robust and are inapplicable to practical scenarios of low SNR and high stand-off distance. Recently, we discussed how one can pose this inversion as a general image restoration problem and hence utilize a Plug-and-Play (PnP) image reconstruction framework which allows state-of-the-art reconstruction through denoiser-driven regularization [7] over traditional ones like total-variations (TV) based regularization [8]. Block-matching and 3D filtering (BM3D) [9] on account of its robust performance in image denoising tasks has emerged as a well-suited denoiser as a prior in the 2D current reconstruction from magnetic field maps using a quantum sensor [8].

Traditionally, due to the prevalence of Superconducting Quantum Interference Device (SQUID) and other scalar magnetometers, regularized current reconstruction is carried out with only the perpendicular component of the magnetic field (B_z). Using stream flow function ($\boldsymbol{g} = g\vec{z}$ s.t. $\boldsymbol{J} = \nabla \times \boldsymbol{g}$), (4) can be converted to a simpler convolution equation $B_z = \mathcal{M} * g$ where $\mathcal{M}$ is the corresponding kernel but involves an unstable retrieval of current densities due to derivative operation [6]. As also discussed in [4], [5], B_z deconvolution is insufficient for an exact solution as DC components of the $\boldsymbol{J}$ are undetermined and cannot be reconstructed from the measured B_z map. Since the path also involves singularities, deconvolving only using B_z is observed to produce artifacts in the reconstruction [2]. With the power of newly emerging vector magnetometry, where all three components of the magnetic field $\boldsymbol{B}$ in the lab frame can be measured, one can provide more information for reconstruction [5], [10].

Here, we propose a new joint formulation for 2-D current reconstruction integrating both vector magnetometer maps and PnP-based regularizers, working out and adapting each algorithmic step to our problem's context. To mitigate the practical issues discussed above, we introduce a weak coupling through data-fidelity term of B_z along with the continuity term and a regularizer ($\mathcal{R}$) that can act on both the components of $\boldsymbol{J}$ together pertaining to their similar noise and physical characteristics. Considering vector $\boldsymbol{B}$ map in deconvolution can lead to a more physically consistent current reconstruction as the estimated $\boldsymbol{J}$ would properly reproduce whole $\boldsymbol{B}(x,y)$ map instead of just a single component [10]. We employed appropriate boundary conditions to the $\boldsymbol{B}$ maps that can reconstruct $\boldsymbol{J}$ maps consistently using the proposed formulation. This also solves the problem of discontinuities in the reconstructed current density components during independent deconvolution of (2-3), specifically at the corners or splits where each of the components is interdependent by the continuity equation. Our experiments show that the proposed formulation consistently performs better than the previous techniques at critical regions like corners for practically relevant scenarios and can produce a physically closer reconstruction of current maps.

The paper is organized as follows: in Section II, we propose a novel technique that jointly solves for the 2-D current reconstruction problem for vector current density maps. Such an approach does not exist in the context of the addressed problem to the best of our knowledge. The relevant results captured in Section III demonstrate the applicability and usefulness of the technique, including an essential improvement in reconstruction quality compared to the existing method on real data. It is followed by concluding remarks in Section IV.

II. Proposed Method

We aim to deconvolve current densities jointly using the following forward problem:

$$\begin{aligned}\underset{J_x,J_y}{\operatorname{argmin}}\ & \frac{w_1}{2}\left\|B_x - G_3 * J_y\right\|_2^2 \\ &+ \frac{w_2}{2}\left\|B_y + G_3 * J_x\right\|_2^2 \\ &+ \frac{w_3}{2}\left\|B_z - G_1 * J_x + G_2 * J_y\right\|_2^2 \\ &+ \lambda_1\left\|D_x * J_x + D_y * J_y\right\|_2^2 \\ &+ \lambda_2\mathcal{R}\left(J_x, J_y\right)\end{aligned} \tag{6}$$

Here, the first three terms are data-fidelity terms that try to model the current flow such that it will produce the measured magnetic field. The fourth term enforces the continuity equation ($\nabla.\vec{J} = \partial_x J_x + \partial_y J_y = 0$), ensuring the absence of sources or sinks of current flow. Here, $D_x, D_y \in \mathbb{R}^{N\times N}$ are matrices encoding the finite differences operator [6]. Numerically, this condition of a physical current flow is hard to get satisfied because of which it is added as a regularizer, providing a relaxation in the optimization process. $\mathcal{R}\left(J_x, J_y\right)$ corresponds to an extra regularizer that is needed to characterize the current density reconstruction and further constrain the solution space. Additionally, we used efficient variable splitting methods like

Noise levels	z_0 (μm)	Deconvolution Approaches								
		Proposed Joint Deconvolution			Using parallel components			Using perpendicular component		
		S1	S2	S3	S1	S2	S3	S1	S2	S3
30 dB	7	28.9, 0.96	27.2, 0.85	19.5, 0.87	26.2, 0.92	24.5, 0.72	19.7, 0.87	22.6, 0.23	20.6, 0.29	12.3, 0.12
	21	23.2, 0.87	21.2, 0.48	13.8, 0.64	22.8, 0.76	20.1, 0.48	13.9, 0.61	19.8, 0.17	19.0, 0.21	9.9, 0.10
20 dB	7	28.1, 0.85	25.6, 0.58	19.4, 0.53	25.5, 0.83	23.8, 0.49	19.3, 0.58	20.4, 0.30	22.1, 0.36	9.9, 0.07
	21	22.1, 0.79	20.1, 0.42	12.2,0.34	21.8, 0.78	20.4, 0.48	12.7, 0.35	19.4, 0.15	19.7, 0.30	9.9, 0.05

TABLE I: Comparison of performance of proposed Joint Deconvolution in terms of PSNR and SSIM.

alternating direction method of multipliers (ADMM) [11] for solving this complex, high-dimensional optimization problem.

A. Algorithmic steps for optimization

The optimization problem (6) can be written in standard ADMM form as

$$\begin{aligned}\underset{J_x,J_y}{\operatorname{argmin}} \quad & \frac{w_1}{2}\left\|B_x-\hat{G}_3J_y\right\|_2^2+\frac{w_2}{2}\left\|B_y+\hat{G}_3J_x\right\|_2^2 \\ & +\frac{w_3}{2}\left\|B_z-\hat{G}_1J_x+\hat{G}_2J_y\right\|_2^2+\lambda_1\left\|Z_{1_x}+Z_{1_y}\right\|_2^2 \\ & +\lambda_2\mathcal{R}\{Z_{2_x},Z_{2_y}\} \\ & \text{s.t.}\begin{pmatrix}\hat{D}_xJ_x\\ \hat{D}_yJ_y\\ J_x\\ J_y\end{pmatrix}=\begin{pmatrix}Z_{1_x}\\ Z_{1_y}\\ Z_{2_x}\\ Z_{2_y}\end{pmatrix}\end{aligned} \tag{7}$$

where $\hat{}$ denotes the convolution matrix corresponding to its respective kernel, $\boldsymbol{J}=(J_x,J_y)$ and $\boldsymbol{Z}=(Z_{1_x},Z_{1_y},Z_{2_x},Z_{2_y})$ are auxiliary variables and $\boldsymbol{U}=(U_{1_x},U_{1_y},U_{2_x},U_{2_y})$ will be dual variable. It is to be noted that all variables are vectorized accordingly in the context of (7). Following standard ADMM procedure [7], an augmented Lagrangian $\mathcal{L}_\rho(\boldsymbol{J},\boldsymbol{Z},\boldsymbol{U})$ can be derived from our separated optimization sub-problems (7) so that $\boldsymbol{J}$ and $\boldsymbol{Z}$ can be optimized alternatively.

We get closed form solutions for $\boldsymbol{J}$ proximal operator:

$$\boldsymbol{J}^{(k+1)}=\underset{\boldsymbol{J}}{\operatorname{argmin}}\,\mathcal{L}_\rho(\boldsymbol{J},\boldsymbol{Z}^{(k)},\boldsymbol{U}^{(k)}) \implies$$

$$J_x^{(k+1)}=\mathcal{F}^{-1}\left[\frac{\begin{array}{r}-w_1g_3^*b_y+w_3(g_2^*b_z+g_2^*g_1j_y^{(k)})+\\ \rho\left(d_x^*(z_{1_x}-u_{1_x})+z_{2_x}-u_{2_x}\right)\end{array}}{w_2g_3^*g_3+w_3g_1^*g_1+\rho(d_x^*d_x+1)}\right] \tag{8}$$

$$J_y^{(k+1)}=\mathcal{F}^{-1}\left[\frac{\begin{array}{r}w_1g_3^*b_x-w_3(g_2^*b_z-g_2^*g_1j_x^{(k)})+\\ \rho\left(d_y^*(z_{1_y}-u_{1_y})+z_{2_y}-u_{2_y}\right)\end{array}}{w_1g_3^*g_3+w_3g_2^*g_2+\rho(d_y^*d_y+1)}\right] \tag{9}$$

where lower-case symbols represent respective 2-D discrete fourier variables and $*$ denotes the complex conjugate operation on matrices. Using these expressions for $\boldsymbol{J}$ update brings instabilities because of contribution of initialized $J_x(J_y)$ in $J_y(J_x)$ update coming from B_z relation (4). Hence, a slight modification can be done in the update by considering (8) and (9) as a system of linear equations in two variables and eliminating the other variable from the respective equation. This is equivalent to saying that rather than alternately minimizing $\mathcal{L}_\rho$, we are solving simultaneously for both the primal variables (J_x and J_y) in a single step. Due to now decoupled update of these primal variables, we observed a stable solution even after incorporating contributions from B_z, making it equivalent to the stream flow deconvolution [6] without facing issues that can arise while taking derivatives [4].

Similarly, for $\boldsymbol{Z}$ update:

$$\boldsymbol{Z}^{(k+1)}=\arg\min_{\boldsymbol{Z}}\mathcal{L}_\rho(\boldsymbol{J}^{(k+1)},\boldsymbol{Z},\boldsymbol{U}^{(k)}) \implies$$

$$Z_{1_x}^{(k+1)}=\mathcal{F}^{-1}\left[\frac{-z_{1_y}^{(k)}+\rho/\lambda_1(d_xj_x^{(k+1)}+u_{1_x}^{(k)})}{1+\rho/\lambda_1}\right] \tag{10}$$

$$Z_{1_y}^{(k+1)}=\mathcal{F}^{-1}\left[\frac{-z_{1_x}^{(k)}+\rho/\lambda_1(d_yj_y^{(k+1)}+u_{1_y}^{(k)})}{1+\rho/\lambda_1}\right] \tag{11}$$

$$Z_{2_x}^{(k+1)}=\mathcal{R}_{\lambda_2/\rho}\left(J_x^{(k+1)}+U_{2_x}^{(k)}\right) \tag{12}$$

$$Z_{2_y}^{(k+1)}=\mathcal{R}_{\lambda_2/\rho}\left(J_y^{(k+1)}+U_{2_y}^{(k)}\right) \tag{13}$$

where updates for Z_{2_x} and Z_{2_y} comes directly from denoisers as per PnP framework. The same trick discussed for (8) and (9) can be applied to (10-11), which seems to be a stricter condition leading to faster convergence [4].

Update for scaled dual variables $\boldsymbol{U}$ becomes:

$$\boldsymbol{U}^{(k+1)}=\underset{\boldsymbol{U}}{\operatorname{argmin}}\,\mathcal{L}_\rho(\boldsymbol{J}^{(k+1)},\boldsymbol{Z}^{(k+1)},\boldsymbol{U}) \implies$$

$$U_{1_x}^{(k+1)}=U_{1_x}^{(k)}+\mathcal{F}^{-1}\left\{d_1j_x^{(k+1)}\right\}-Z_{1_x}^{(k+1)} \tag{14}$$

$$U_{1_y}^{(k+1)}=U_{1_y}^{(k)}+\mathcal{F}^{-1}\left\{d_2j_y^{(k+1)}\right\}-Z_{1_y}^{(k+1)} \tag{15}$$

$$U_{2_x}^{(k+1)}=U_{2_x}^{(k)}-Z_{2_x}^{(k+1)} \tag{16}$$

$$U_{2_y}^{(k+1)}=U_{2_y}^{(k)}-Z_{2_y}^{(k+1)} \tag{17}$$

These optimization steps ((8)-(17)) are iterated over until residual ($R^{(k+1)}=||\boldsymbol{J}^{(k+1)}-\boldsymbol{J}^{(k)}||_2^2+||\boldsymbol{Z}^{(k+1)}-\boldsymbol{Z}^{(k)}||_2^2+||\boldsymbol{U}^{(k+1)}-\boldsymbol{U}^{(k)}||_2^2$) is below an empirically pre-determined threshold $\epsilon>R^{(K)}$.

B. Tackling outside the field of view

Another complication arises from the long-range nature of current-induced magnetic fields in the reconstruction [4], [5]. In order to obtain an accurate solution, one must make assumptions about the behaviour of the current outside the measurement window. Traditional symmetric padding leads to different current directions at the same boundary from different B-maps when considered together for joint deconvolution due

to directionality in the magnetic field components. Instead, one can use a more natural boundary condition for each component of magnetic field such that the current flow is continuous and consistent with other components of magnetic field. Hence, we apply the following boundary conditions [4]:

$$B_x(x,y) = +B_x(-x,y);\ B_x(x,y) = -B_x(x,-y) \quad (18)$$

$$B_y(x,y) = -B_y(-x,y);\ B_y(x,y) = +B_y(x,-y) \quad (19)$$

$$B_z(x,y) = +B_z(-x,y);\ B_z(x,y) = +B_z(x,-y) \quad (20)$$

III. Results and Discussion

In this section, the potential of the proposed joint formulation is quantitatively demonstrated while considering three simulated geometries, encompassing identified critical scenarios, of area $110 \times 110\ \mu m^2$, feature size $8\ \mu m$ and $I = 600\ \mu A$. Particularly, three characteristics are simulated (Fig. 1a): i) a bent wire (S1), ii) a circular coil (S2) with radius of $40\ \mu m$, and iii) two straight wires (S3) separated by $8\ \mu m$ with current flowing in the same direction. The sensor is assumed to have a pixel size of $\Delta x = 1\ \mu m$, resulting $N = L/\Delta x = 110$. $\boldsymbol{J}$ maps for each geometry is generated using COMSOL multiphysics [12] on a regular grid. It is to be noted that a relatively stable forward relations (2-4) is employed to calculate $\boldsymbol{B}$ at $z_0 = 7\ \mu m$ and $21\ \mu m$ in the DFT domain. Simulated Gaussian noise with zero mean was added to have a target Peak Signal-to-Noise Ratio (PSNR) of 30 dB and 20 dB for the resulting $\boldsymbol{B}$ map. Quantitative analysis of estimation of each of these geometries can be done using relevant quantities like the estimated total current amplitude (I) along with PSNR and structural similarity index measure (SSIM) for fine-grained evaluation.

A summary of the typical results obtained is given in Table I where PSNRs and SSIMs of the reconstructed $||\boldsymbol{J}||_2$ are calculated for proposed joint approach and other two approaches using only parallel components [8] and using perpendicular component (adapted from [4] and [6]). Estimated $\boldsymbol{J}$ maps obtained for the extreme case of $z_0 = 21\ \mu m$ and PSNR = 20 dB are also shown in Fig. 1. We found the proposed approach to be quantitatively superior for all the geometries consistently while achieving the goal of more physical reconstructions. It should be noted that the problem with just using B_z directly to reconstruct $\boldsymbol{J}$ is the resultant unknown offset in the mean value of current amplitude [4]. One workaround of this problem can be the subtraction of the mean value of each component of $\boldsymbol{J}$, which may lead to other artifacts and incorrect amplitude as shown in Fig. 1e. Table I gives a clear picture that it is easier to produce isolated rectilinear geometries than circular coils, which could be due to the unsuitable grid. Notice in Table I and in Fig. 1 a poor performance when deconvolving B_z with straight wires, which happened due to the unresolved current-carrying wires.

A. Reconstruction with experimental data

We obtained B_z experimentally using a wide-field quantum diamond microscope of a coil sample having the same specifications as that of the simulated case but with a feature size of $2\ \mu m$ at $z_0 = 7\ \mu m$ [13]. Parallel components (B_x and B_y) are obtained using the relations in the DFT domain in a charge-free region [10] that are shown in Fig. 2a. Estimated current density through different routes is shown in Fig. 2b-Fig.2h. Notice a better reconstruction at the corner of coils and regions just around the coil (critical regions) in Fig. 2d through our proposed joint deconvolution from reconstruction through parallel components independently (Fig. 2e; [8]) or just through perpendicular component (Fig. 2g, equivalent to

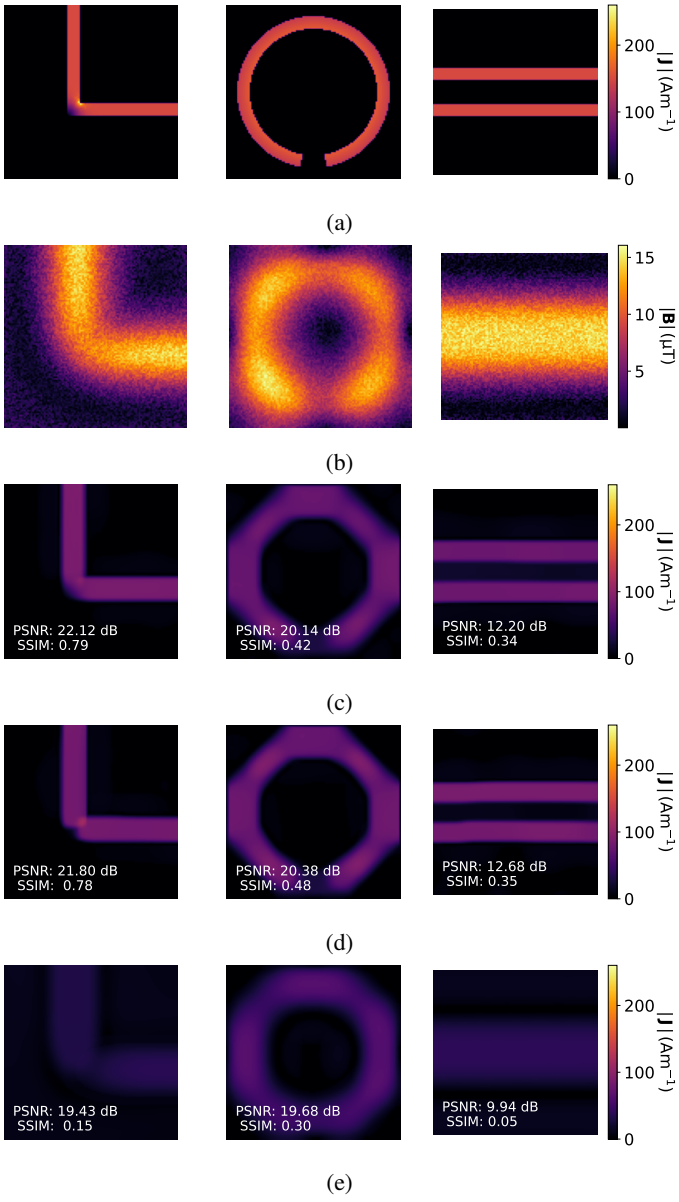

Fig. 1: (a) J maps of simulated geometries: S1, S2 and S3 respectively. (b) Magnetic field maps obtained from forward model at $z_0 = 21\ \mu m$ having PSNR = 20 dB. Notice, two straight wires are not resolvable visibly in magnetic maps. We showed estimated current density with (c) proposed joint formulation, (d) using only parallel components or (e) using just the perpendicular component, respectively.

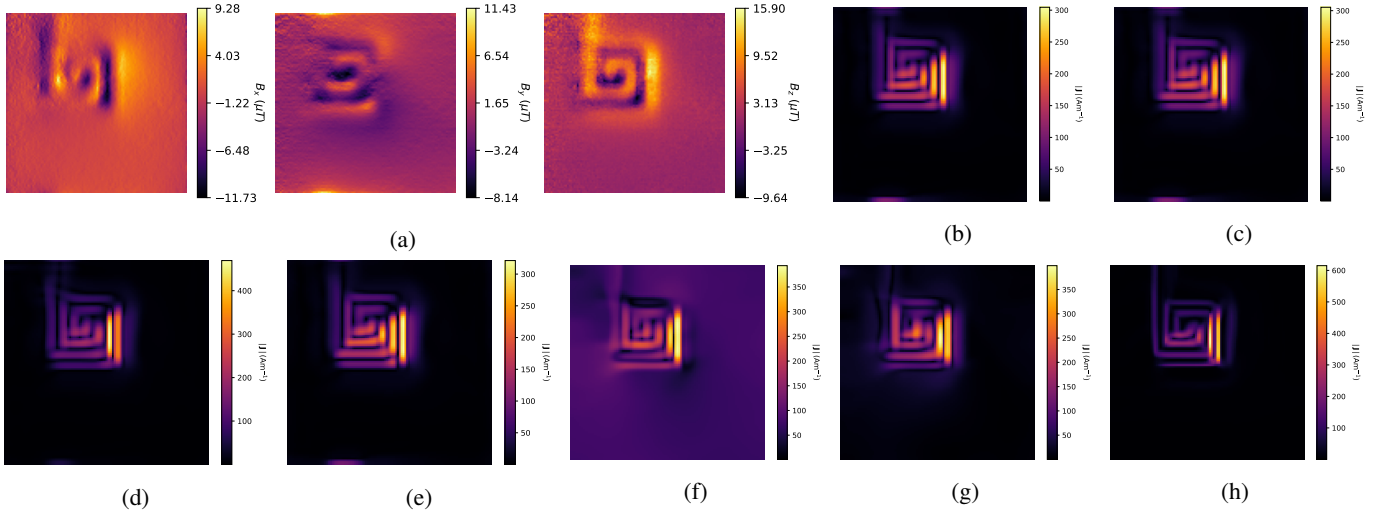

Fig. 2: (a) Experimentally measured maps of $\boldsymbol{B}$ Components [10], (b) Joint-Estimation of $|\boldsymbol{J}|$ with only $w_3 = 0.0$, (c) Joint-Estimation of $|\boldsymbol{J}|$ with only $w_3 = 0.01$, (d) Joint-Estimation of $|\boldsymbol{J}|$ with $w_1 = w_2 = w_3 = w_4 = 1.$, (e) Separate-Estimation of J_y, J_x from just B_x and B_y, (f) Joint-Estimation of $|\boldsymbol{J}|$ with $w_1 = w_2 = 0.0$, (g) Corrected Joint-Estimation of $|\boldsymbol{J}|$ with $w_1 = w_2 = 0.0$ [4] and (h) Estimation of $|\boldsymbol{J}|$ through stream-flow function $\boldsymbol{g}$ [6]

[4]) or via stream-flow function (Fig. 2h; [6]). Again, we subtracted the mean values of current maps from them to solve the problem in Fig. 2f to obtain the current map in Fig. 2g. On the other hand, Fig. 2h shows an excellent noise suppression, but the known problem of instabilities due to derivative operation gives very high unphysical current amplitudes in the reconstruction. Different weights of the data-fidelity term essentially implies different optimization problems, and the exact combination of weights depend on the goal of the problem. Therefore, we present the current estimation with three different weights to the data-fidelity term corresponding to B_z in Fig. 2b, 2c, and 2d.

IV. Conclusions

In this paper, estimating current density images in two dimensions from magnetic field images measured at a distance from the source is attempted. A joint deconvolution problem is formulated within an optimization framework, employing contemporary signal processing techniques. The suggested technique can be used for different applications and can contribute to advances in signal processing in the important field of quantum sensing. The proposition negotiates the difficulty of direct deconvolution and also can accommodate additional noise/artifacts for future extensions. Further enhancements to minimize errors caused by kernel mismatch, due to wrong or lack of knowledge of the stand-off distance, is one such direction. Parametrizing Green function filters, enhancing reconstruction by employing trained deep learning priors/denoisers for magnetic sensing, can be explored as well.

References

[1] Jeronimo R Maze, Paul L Stanwix, James S Hodges, Seungpyo Hong, Jacob M Taylor, Paola Cappellaro, Liang Jiang, MV Gurudev Dutt, Emre Togan, AS Zibrov, et al. Nanoscale magnetic sensing with an individual electronic spin in diamond. *Nature*, 455(7213):644–647, 2008.

[2] Marwa Garsi, Rainer Stöhr, Andrej Denisenko, Farida Shagieva, Nils Trautmann, Ulrich Vogl, Badou Sene, Florian Kaiser, Andrea Zappe, Rolf Reuter, and Jörg Wrachtrup. Three-dimensional imaging of integrated-circuit activity using quantum defects in diamond. *Phys. Rev. Appl.*, 21:014055, Jan 2024.

[3] Prabhat Anand, Ankit Khandelwal, Achanna Anil Kumar, M Girish Chandra, Pavan K Reddy, Anuj Bathla, Dasika Shishir, and Kasturi Saha. Phase-based approaches for rapid construction of magnetic fields in nv magnetometry. *IEEE Sensors Letters*, 9(3):1–4, 2025.

[4] Alexander Y. Meltzer, Eitan Levin, and Eli Zeldov. Direct reconstruction of two-dimensional currents in thin films from magnetic-field measurements. *Phys. Rev. Appl.*, 8:064030, Dec 2017.

[5] D.A. Broadway, S.E. Lillie, S.C. Scholten, D. Rohner, N. Dontschuk, P. Maletinsky, J.-P. Tetienne, and L.C.L. Hollenberg. Improved current density and magnetization reconstruction through vector magnetic field measurements. *Phys. Rev. Appl.*, 14:024076, Aug 2020.

[6] Colin B. Clement, James P. Sethna, and Katja C. Nowack. Reconstruction of current densities from magnetic images by bayesian inference, 2021.

[7] Suhas Sreehari, S. V. Venkatakrishnan, Brendt Wohlberg, Gregery T. Buzzard, Lawrence F. Drummy, Jeffrey P. Simmons, and Charles A. Bouman. Plug-and-play priors for bright field electron tomography and sparse interpolation. *IEEE Transactions on Computational Imaging*, 2(4):408–423, 2016.

[8] Prabhat Anand, Anuj Bathla, Pavan K Reddy, Ankit Khandelwal, M Girish Chandra, and Kasturi Saha. On robust 2d current reconstruction in quantum diamond magnetometry. In *CLEO 2025*. Optica Publishing Group, 2025, in press.

[9] K. Dabov, A. Foi, V. Katkovnik, and K. Egiazarian. Image denoising by sparse 3-D transform-domain collaborative filtering. *IEEE Trans. Img. Process.*, 16(8):2080–2095, 2007.

[10] Eduardo A. Lima and Benjamin P. Weiss. Obtaining vector magnetic field maps from single-component measurements of geological samples. *Journal of Geophysical Research: Solid Earth*, 114(B6), 2009.

[11] S. Boyd, N. Parikh, E. Chu, B. Peleato, J. Eckstein, et al. Distributed optimization and statistical learning via the alternating direction method of multipliers. *Found. Trends in Mach. learn.*, 3(1):1–122, 2011.

[12] COMSOL Multiphysics. Introduction to comsol multiphysics®. *COMSOL Multiphysics, Burlington, MA, accessed Feb*, 9:2018, 1998.

[13] Madhur Parashar, Anuj Bathla, Dasika Shishir, Alok Gokhale, Sharba Bandyopadhyay, and Kasturi Saha. Sub-second temporal magnetic field microscopy using quantum defects in diamond. *Scientific Reports*, 12(1):8743, May 2022.